Study of surface cracking during extrusion of aluminium alloy AA 2014

Z. Peng and T. Sheppard

Surface cracking is generally recognised as one of the main defects occurring during the process of aluminium extrusion, especially in the case of the so called hard aluminium alloys. Previous experiments suggest that this type of defect is caused by the rise in temperature as the process proceeds. Some experiments indicate that the surface quality is good even though the temperature may be high during extrusion. It is also well known that crack criteria have been adopted to explain the cracking that occurs in extrusion, blanking and rolling, etc. In this study, a finite element method (FEM) is used in different ways to predict surface cracking during hot extrusion. The crack criteria are integrated into the FEM code FORGE®2.0. The effectiveness of these criteria in predicting surface cracking in the case of hot extrusion is discussed. The FEM simulation also provides some other quantitative data, such as the temperature rise during extrusion from different initial temperatures. In addition, the principal stresses at the die land area at different extrusion stages are also shown. **MST/5986**

Keywords: Aluminium alloys, Extrusion, Defects, Surface cracking

The authors are at DEC, Bournemouth University, 12 Christchurch Road, Bournemouth, UK, BH1 3NE (tsheppar@bournemouth.ac.uk). *Manuscript received 22 September 2003; accepted 5 February 2004.*

Introduction

Al–Cu–Mg alloy systems have been in use since their discovery over half a century ago. The development of AA 2014 alloy utilised the effect of silicon to produce an Al–Cu–Mg alloy that is more susceptible to artificial aging than 2017, and provides a high level of strength unobtainable in naturally aged 2017. This alloy has widespread applications in the aircraft industry. The chemical composition limits for 2014 are shown in Table 1.

Copper is one of the most important alloying constituents for aluminium because of its appreciable solubility and strengthening effect, the strength increasing with increasing copper content up to a maximum of approximately 6%. Magnesium is used in combination with copper to accelerate and increase age hardening at room temperature. The equilibrium compounds for this system are $CuAl_2$ (θ phase) and $CuMgAl_2$ (S phase).[1,2] These are soluble in the matrix during solution heat treatment.

During extrusion, imperfections in the quality of the extrudate may arise, ranging from a rough or uneven surface to complete disintegration of the extrudate. The surface finish of the product is as important as the mechanical properties, and the control of defects is often the deciding factor in determining the extrusion conditions. Defects that may occur vary from visible blemishes such as cracks, blisters, and die lines, to invisible ones that show up after anodising. While in high strength aluminium alloys where die lines and surface scoring have only secondary importance to the mechanical property requirements (because the surface often has to be machined to remove recrystallised layers) the defect is tolerated provided the die lines are not so coarse that stress concentrations arise.[3] For 4%Cu alloys, surface cracking (or speed cracking) is a major problem, especially at high temperatures and strain rates. Since the product must be scrapped due to poor surface quality and inferior mechanical properties, it is of primary importance to study the occurrence of surface cracking in the extrusion of hard alloys.

In order to evaluate surface cracking, extrusions have been placed into one of three categories:[3]

A – no evidence of cracking

B – cracking commences at some distance along the extrudate

C – Cracking occurs along the entire length of the extrudate increasing in severity as extrusion proceeds

Typical examples of these three categories are shown in Fig. 1, all taken from the same position half way along the extruded length at $0{\cdot}5L$.

Historically a trial and error method has been used to form extrusion products of sufficient quality, a costly, uncertain, and time consuming practice. The ability to identify and predict these defects is critical to modern practice and is challenging fundamentally. Recently, the development and application of numerical techniques, such as the finite element method (FEM), to continuum mechanics problems has provided a powerful facility to solve this problem.

A typical simulation procedure carried out by FEM, can consider the effect of:

(i) the geometry of the die and workpiece;

(ii) operating variables such as temperature and the rate of deformation, the bulk constitutive response of the material, and the interaction with solid boundaries.

(iii) Stresses and strains are then calculated as functions of time, from which predictions regarding the occurrence of fractures are obtained.

Cracking criteria

There exist a number of criteria for assessing rupture in metal forming process,[4,5] which are based on experimental work that utilises a deformation process related to actual industrial applications. The initiation of ductile fracture in

Table 1 Chemical compostion of AA 2014 (balance Al)

Si	Fe	Cu	Mn	Mg	Cr	Zn	Ti
0·50–1·2	0·7	3·9–5·0	0·40–1·2	0·20–0·8	0·10	0·25	0·15

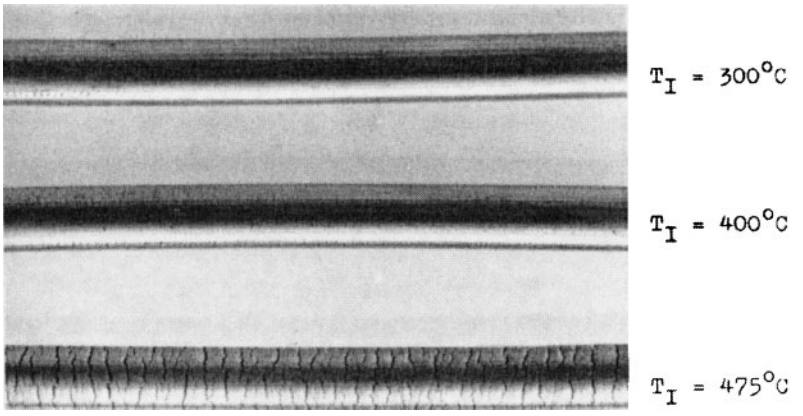

1 Three categories of surface cracking

metals depends strongly on the stress and strain histories. Many ductile fracture criteria have the form that fracture occurs when the value of a damage parameter, which is given as an integral form of stress and strain, reaches a particular value. In this study, several of the criteria were combined into the FEM subroutine to see if there was a critical value to indicate the initiation of surface cracking in hot extrusion. The details of the selected criteria are:

(1) Oyane

$$\int_0^{\varepsilon_R} \left(1 + A\,\frac{\sigma_H}{\sigma_{eq}}\right) d\varepsilon_{eq} \geqslant C1 \quad \ldots\ldots\ldots (1)$$

where A and $C1$ are constants, σ_H is the hydrostatic stress, σ_{eq} is the equivalent stress, ε_{eq} is the equivalent strain. The process by which fractures occur in metal forming has been widely modelled as void initiation and growth, followed by coalescence to form a crack. Based on this hypothesis, criteria for ductile fracture have been suggested by McClintock *et al.*[6] and Oyane *et al.*[7]

(2) Cockroft and Latham (C–L1)

$$\int_0^{\varepsilon_R} \sigma^*\, d\varepsilon_{eq} \geqslant C2 \quad \ldots\ldots\ldots (2)$$

$$\sigma^* = \mathrm{Max}(\sigma_1,\sigma_2,\sigma_3) \quad \ldots\ldots\ldots (3)$$

where $C2$ is a constant, σ^* is the maximum principle stress. Cockcroft and Latham[8] considered the effects of the maximum principal tensile stress over the plastic strain path to fracture.

(3) Cockroft and Latham normalised (C–L2)

$$\int_0^{\varepsilon_R} \frac{\sigma^*}{\sigma_{eq}}\, d\varepsilon_{eq} \geqslant C3 \quad \ldots\ldots\ldots (4)$$

where $C3$ is a constant. This criterion has a dependence on hydrostatic stress.

(4) Ayada

$$\int_0^{\varepsilon_R} \left(\frac{\sigma_H}{\sigma_{eq}}\right) d\varepsilon_{eq} \geqslant C4 \quad \ldots\ldots\ldots (5)$$

where $C4$ is a constant.

(5) Generalised work criterion (GW) or Freudenthal criterion

$$\int_0^{\varepsilon_R} \sigma_{eq}\, d\varepsilon_{eq} \geqslant C5 \quad \ldots\ldots\ldots (6)$$

or

$$\int_0^{\varepsilon_R} (\sigma_1\dot{\varepsilon}_1 + \sigma_2\dot{\varepsilon}_2 + \sigma_3\dot{\varepsilon}_3) \geqslant C5' \quad \ldots\ldots\ldots (7)$$

where $C5$ and $C5'$ are constants.σ_1, σ_2, and σ_3 are the principle stresses and $\dot{\varepsilon}_1$, $\dot{\varepsilon}_2$, and $\dot{\varepsilon}_3$ are the corresponding principle strain rates.

Freudenthal[9] proposed that energy is the critical parameter at fracture. With this criterion, fracture occurs in a material element when the rate of plastic energy dissipation reaches a critical value when integrated with respect to time, following the element as it travels through the die. This is the only criterion that accurately predicted the site of fracture initiation for all three metal forming processes considered: upsetting, extrusion (brass), and strip deformation in the work of Clift *et al.*[5]

(6) Temperature

$$T \geqslant C6 \quad \ldots\ldots\ldots (8)$$

where $C6$ is a constant. If the heat generation near the die land area increases the local temperature such that the applied stresses exceed the resistance to deformation then severe cracking at the surface may be expected. This temperature generation is a function of the alloy chemistry, extrusion speed, extrusion ratio, aspect ratio, container temperature, and initial billet temperature.[3] Much of the heat generated at the surface occurs through the dead metal zone and the deformation zone shear band, which terminates on the face of the die immediately ahead of the die land area. This results in a steep rise in the temperature as the material approaches the die land.[10] Heat generation is comparatively less in the indirect mode of extrusion compared to the direct mode.

According to the six criteria described above, when the constants $C1-C6$ reach a critical value, the crack occurs.

By integrating the crack criteria into FEM programs, research has been carried out to study various criteria adopted in metal forming processes.

Hambli and Reszka[4] checked fracture criteria validity using an FEM model of the blanking operation by an inverse technique approach. Their study showed that valid critical values for crack initiation by shearing mechanisms could be predicted by the following fracture criteria: Rice, Freudenthal, Cockroft and Latham, Atkins, Oyane, Ayada, and plastic strain.

Clift *et al.*[5,11] described the use of the finite element technique to predict fracture initiation in a range of simple metal forming operations, which included simple upsetting, axisymmetric extrusion, and strip compression and tension. In the case of axisymmetric extrusion, their study showed that numerically predicted sites of fracture agreed with experiment when the Oyane, Freudenthal, and C–L criteria were adopted. However, the extrusion ratio was very small in their study and the influence of temperature rise, which is a very important factor for crack initiation during extrusion, was again ignored.

In the work of Ko *et al.*,[12] The C–L criterion was adopted for FEM simulation and it was confirmed to be valid for predicting crack initiation during aluminium

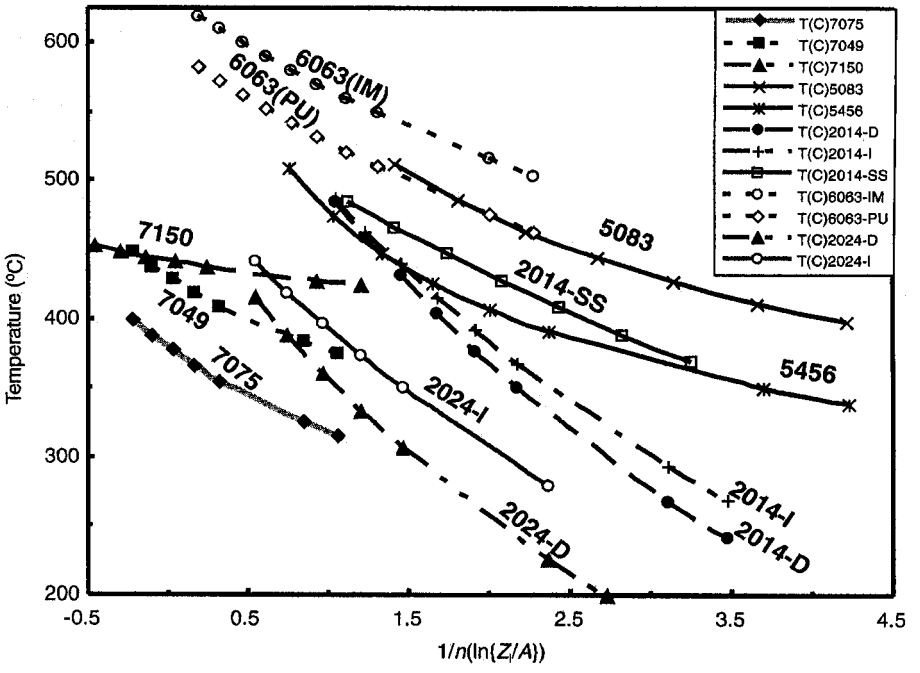

2 Extrusion limit

extrusion. However, the extrusion ratio used was also very small and the temperature rise was not studied.

It is interesting to see that some studies on paste extrusion, which can be assumed to be a real isothermal process, have been performed by Domanti *et al.*[13] The C–L criterion and the generalised work criterion are discussed in their study, and these criteria are shown to be successful in predicting the increase in fracture with increasing die entry angle. They are also proved to be at least qualitatively correct in considering the effect of extrusion ratio on surface fracture. Domanti *et al.*'s work is an ideal example of an isothermal extrusion, which can be contrasted with the present work, in which the temperature evolution has to be involved.

Some investigations[3,4,12] have shown that it is difficult to choose a fracture criterion that is 'universal' enough in the sense that it gives consistent results for operating conditions outside the calibration range. Applications of critical values of fracture criteria are only successful when they are both characterised and applied under similar loading conditions. A material might crack at a relatively small deformation during forging, yet might be satisfactorily deformed to a very large strain by extrusion. The onset of cracking depends both on the details of the working process to which the material is subjected and on its basic ductility.

In addition to the criteria mentioned above, there also exists an empirical method to predict surface cracking occurring in hot extrusion, proposed by Sheppard and Tutcher.[14] They investigated the incidence of speed cracking in the rod form of AA 5456 alloy and showed that the Z parameter may be used to correlate results over widely varying temperature and speed conditions.

For acceptable surface quality

$$\ln\left(\frac{Z_i}{A}\right) \leqslant \frac{6{\cdot}35\times10^{20}}{T_i^{7{\cdot}06}} \quad \ldots\ldots\ldots\ldots (9)$$

where Z_i is the Zener–Holloman parameter using the average strain rate and the initial temperature

$$Z_i = \dot{\bar{\varepsilon}} \exp(Q/RT_i) \quad \ldots\ldots\ldots\ldots (10)$$

$\dot{\bar{\varepsilon}}$ is the average strain rate, defined by

$$\dot{\bar{\varepsilon}} = \frac{6D_B^2 v(a+b\ \mathrm{Ln}\ R)(C+\mathrm{d}\ \mathrm{Tan}\ \omega)}{D_B^3 - D_E^3} \quad \ldots\ldots (11)$$

D_B is the billet diameter, D_E is the extrudate diameter, v is the ram speed, R is the extrusion ratio, ω is the deformation zone cone semi-angle,[1] which is defined by

$$\omega = 38{\cdot}7 - 6{\cdot}9\ \mathrm{Ln}\ R \quad \ldots\ldots\ldots\ldots (12)$$

a, b, c, and d are constants ($a=0{\cdot}171$, $b=1{\cdot}86$, $c=38{\cdot}7$, $\mathrm{d}=6{\cdot}9$).[10] T_i is the initial temperature.

This type of analysis has also been applied to the observed surfaces of shaped extrusions in 2024 alloy,[1] and introducing the λ^2 modification for shaped extrusions, acceptable surfaces were achieved when

$$\frac{1}{n}\ln\left(\lambda^2\frac{Z_i}{A}\right) \leqslant \frac{2{\cdot}113\times10^9}{T_i^{2{\cdot}866}} \quad \ldots\ldots\ldots\ldots (13)$$

for direct extrusion and

$$\frac{1}{n}\ln\left(\lambda^2\frac{Z_i}{A}\right) \geqslant \frac{2{\cdot}113\times10^9}{T_i^{2{\cdot}866}} \quad \ldots\ldots\ldots\ldots (14)$$

for indirect extrusion. λ is the shape factor.

These criteria are shown in Fig. 2 for a number of Al alloys.

In the case of 2014 extrusion, Patterson[15] and Vierod[16,17] provided the following empirical criteria:

For direct extrusion, Patterson gave the following equation

$$\ln Z_i \leqslant \frac{6924{\cdot}2}{T_i^{0{\cdot}857}} \quad \text{(correlation: 0·9986)} \quad \ldots\ldots (15)$$

and for indirect extrusion

$$\mathrm{Ln}\ Z_i \frac{15909{\cdot}5}{T_i^{0{\cdot}982}} \quad \text{(Correlation : 0·9991)} \quad \ldots\ldots (16)$$

where T_i is the initial billet temperature in kelvin.

Vierod also reported that different preheat approaches affected this criterion such that for conventional heating (CH, indicating heating continuously to the extrusion temperature)

$$\mathrm{Ln}\ Z_i \frac{67954}{T_i^{1{\cdot}199}} \quad \text{(correlation 0·998)} \quad \ldots\ldots (17)$$

and for material that has been presolution soaked (SS, heat to soak temperature and cool to extrusion

temperature)

$$\text{Ln } Z_i \frac{97955}{T_i^{1\cdot223}} \quad \text{(correlation 0·999)} \quad . \quad . \quad . \quad . \quad . \quad . \quad (18)$$

It can be seen from the above equations that in these empirical equations, only the initial temperature and the average strain rate are considered. With the FE method, the evolution of the instantaneous Zener–Hollomon parameter, in which the real-time strain rate and the real-time temperature are used, can be conveniently obtained from the output program. In this paper, the instantaneous Zener–Hollomon parameter is integrated into the FEM program to observe its evolution during extrusion, and the initial $\text{Ln}Z_i$ and real-time $\text{Ln}(Z_r)$ values are compared. The real-time Zener–Hollomon parameter is defined by

$$Z_r = \dot{\varepsilon} \exp(Q/RT) \quad . \quad . \quad . \quad . \quad . \quad . \quad . \quad . \quad . \quad . \quad . \quad (19)$$

where $\dot{\varepsilon}$ is the real-time strain rate and T is the real-time temperature. With the combination of the initial Z value and the instantaneous Z history, the surface cracking is studied again by the use of the empirical equations.

FEM simulation setting

The main simulation tooling used in this study is shown in Table 2. The billet length was 95 mm and the extrusion ratio 30. Experimental results defining process conditions inducing an unacceptable surface are taken from Refs. 16–19.

The FEM program, FORGE2® was used in this study. It is a process simulation tool based on the finite element method. The hyperbolic sine function was integrated into the FEM to describe material behaviour. The constitutive equation can then be written as

$$\bar{\sigma} = \frac{1}{\alpha} \text{ Ln} \left[\left(\frac{Z}{A} \right)^{\frac{1}{n}} + \left[\left(\frac{Z}{A} \right)^{\frac{2}{n}} + 1 \right]^{\frac{1}{2}} \right] \quad . \quad . \quad . \quad . \quad . \quad (20)$$

where α, A, n are temperature independent constants, $\bar{\sigma}$ is the flow stress, and Z is the Zener–Hollomon parameter. For aluminium alloy AA 2014, $\Delta H = 144{\cdot}408$ kJ mol^{-1}, $\alpha = 0{\cdot}0152$ m^2 MN^{-1}, $n = 5{\cdot}27$, ln $A = 24{\cdot}41$.[16]

Three friction laws are available in FORGE2®: Tresca, viscoplastic, and Coulomb. These three friction laws have been studied by Flitta,[18] who discovered that simulations using the Tresca criterion gave the best result. As a result, only the Tresca law is adopted in this paper. The Tresca friction law is written in the following form

$$\tau = -m \frac{\bar{\sigma}}{\sqrt{3}} \quad . \quad . \quad . \quad . \quad . \quad . \quad . \quad . \quad . \quad . \quad . \quad . \quad (21)$$

where $\bar{\sigma}$ represents the flow stress, m is the friction coefficient, which is in effect a percentage of that which would represent sticking conditions.

Temperature evolution is represented by the following heat equation associated with a certain number of boundary conditions

$$\rho c \frac{dT}{dt} = \text{div}(k \text{ grad}(T)) + \dot{W} \quad . \quad . \quad . \quad . \quad . \quad . \quad . \quad (22)$$

where ρ is the material density, c is the heat capacity, and k is the conductivity.

$\dot{W}$ is the heat power dissipated by plastic deformation, which is written as

$$\dot{W} = \eta \bar{\sigma} \dot{\bar{\varepsilon}} \quad . \quad . \quad . \quad . \quad . \quad . \quad . \quad . \quad . \quad . \quad . \quad . \quad . \quad . \quad (23)$$

The term η represents here the efficiency of the deformation. $\bar{\sigma}$ is the flow stress and $\dot{\bar{\varepsilon}}$ the mean equivalent strain rate.

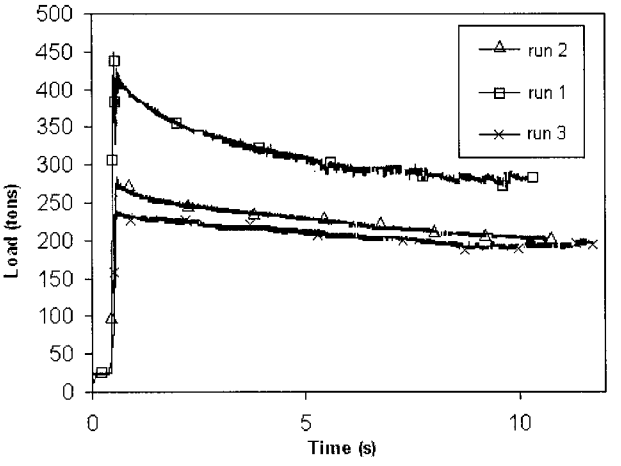

3 Predicted time–load curves

Discussion of simulation results concerning load–time history and temperature evolution

Before we consider the factors affecting surface cracking, the simulation results of load history and temperature evolution must be discussed. Because the strain, the strain rate, and the stress, which are key parameters in the cracking criteria, are closely related to the load and the temperature, it is of primary importance to check the FEM prediction concerning these variables.

Experimental and FEM predicted values of extrusion load are shown in Tables 3 and 4 respectively. The integral file predicted and FEM predicted values of temperature are also shown. Sheppard[19] indicated that there is reasonable agreement between these two calculations, and Dashwood[20] demonstrated that FEM calculations yield results that describe the metallurgical features accurately. Duan and Sheppard[21] demonstrated that the FORGE2 program accurately predicts the temperature throughout rolling pass schedules.

The predicted time–load curves of all the extrusion processes are shown in Figs. 3–5.

Table 2 Tooling of FEM model

Run Code	Extrusion mode	Initial billet temperature, °C	Container temperature, °C	Ram speed, mm s^{-1}	Surface condition
1	Direct	298	275	7·9	A
2	Direct	396	350	7·0	B
3	Direct	470	375	7·3	C
4	Direct	474	430	3·3	B
5	Indirect	464	375	3·4	A

A Surface condition good throughout extrusion.
B Surface cracking occurs from the middle stage of extrusion to the end.
C Surface cracking occurs from the start of extrusion.

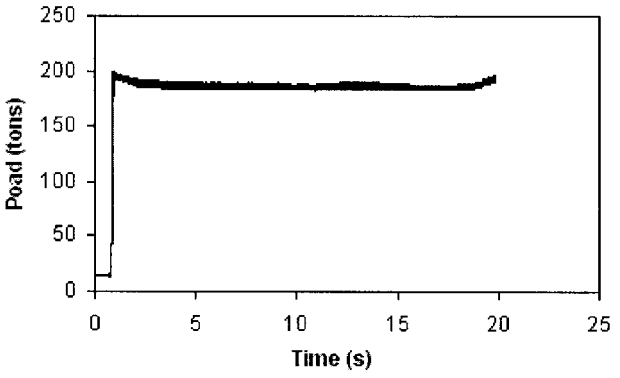

4 Predicted time–load curve of extrusion run 5

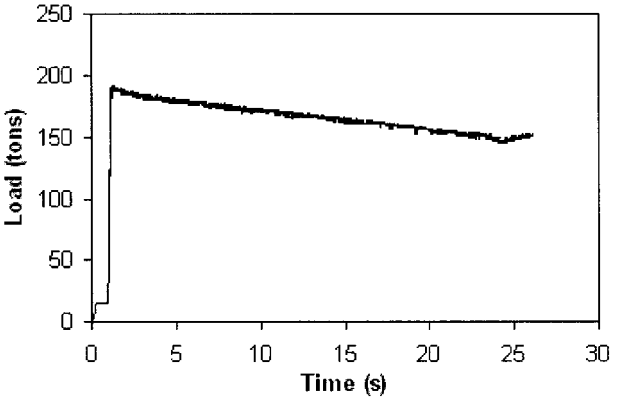

5 Predicted time–load curve of extrusion run 4

In this paper, the data are extracted from two points (side point and centre point) and two lines (AB and CD) at the die land area, as shown in Fig. 6.

The temperature evolution at the side point and centre point of the entire direct extrusion runs are shown in Fig. 7. For the indirect extrusion RUN 5, the positions of the two points were changing throughout the extrusion because they were moving with the die. It is therefore difficult to extract the data continuously as performed for direct extrusions. The temperatures in this case are extracted from line AB at different stages of extrusion, as shown in Fig. 8.

It can be seen clearly that there is a difference between the temperatures at the two points throughout all the extrusion processes. However, at the end of extrusion, the temperature at the centre point rises more quickly than that of the side point and the temperature difference is very small at the end of extrusion. This phenomenon has been reported previously.[22] The difference between the temperature of the extrudate face and centre in this work was close to 30 K, while in Venas's work, the difference was found to be 60 K. Because the billet size used in this study is quite different to that used in Venas's work, it is not strange that there is some discrepancy. The very sharp temperature gradient near the surface is of great significance since it is the surface temperature, and not the average exit temperature, that is critical for surface failure such as cracking.

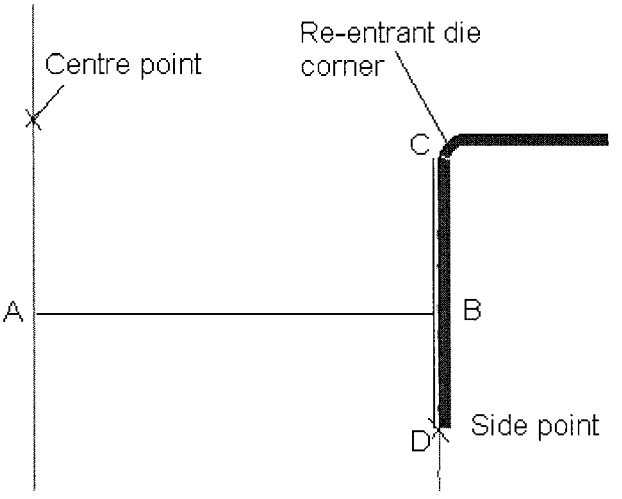

6 Positions of area analysed

Table 3 shows that the predicted loads correlate well with the experimental results. The predicted temperatures, as shown in Table 4, are also in good agreement with the experimental measurements.

It is necessary to point out that the 'cut' technology was adopted in this study. When the material is extruded out of the die to a certain distance, the program deletes the element automatically, as shown in Fig. 9. Figure 9*a* shows an extrusion setting without the 'cut' method, in which all of the elements remain throughout the calculation. It therefore takes an extremely long time to finish a simulation using this approach. However, when the 'cut' technology is used, only a certain length of extrudate remains and the calculation time will be significantly saved, as can be seen from Fig. 9*b*, *c* and *d*. Using this method, all five extrusion processes used in this study were completed within a short time.

It should be noted that in the experiments, if surface cracking occurs it would appear immediately on the surface

Table 3 Load data

Extrusion code	Experimental max load, tons	FEM predicted max load, tons	Experimental min load, tons	FEM predicted min load, tons
1	439·2	445·9	285·8	280·1
2	295·6	286·1	208·6	195·7
3	243·8	240·2	204·6	192·2
4	193·0	190·2	179·3	160·2
5	197·4	203·2	209·7	205·8

Table 4 Temperature

Extrusion code	Peak temp.,* °C	FEM predicted peak temp., °C	Final temp.,* °C	FEM predicted final temp., °C
1	309·1	315·2	470·8	465·7
2	403·5	408·9	501·2	498·2
3	476·1	479·2	546·3	539·6
4	478·0	482·1	529·0	520·4
5	471·3	478·3	488·8	493·2

*Peak temp. is the temperature of the extrudate when the peak load occurs. Both peak temp. and final temp. here are obtained from the integral profile model.

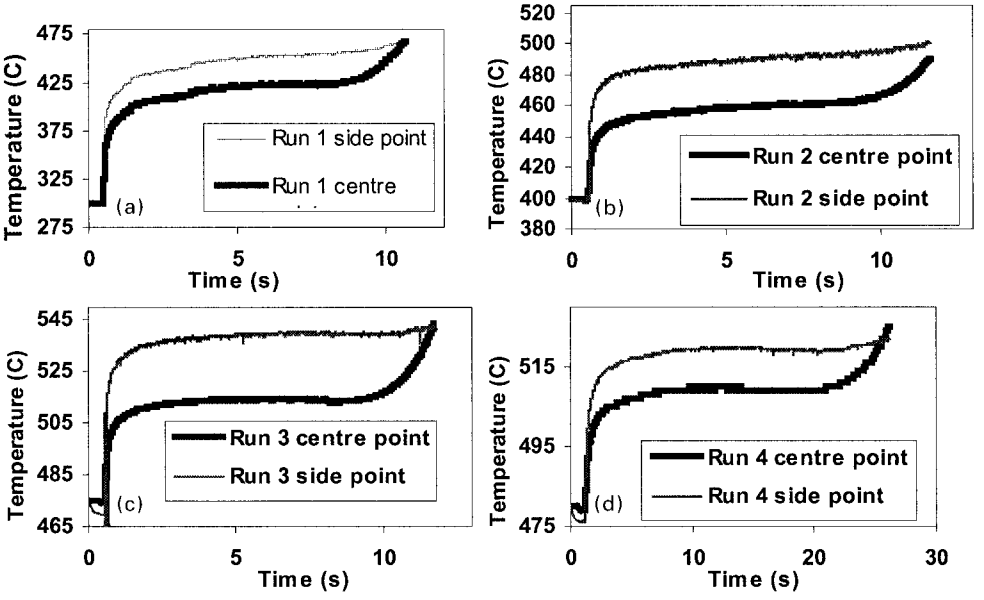

a Run 1; *b* Run 2; *c* Run 3; *d* Run 4

7 Temperature evolution

of the extrudate when it is extruded out of the die. It is therefore evident that more attention should be paid to the die land area while ignoring the stress and strain field at the extrudate far from the die land. When studying surface cracking, the 'cut' technology will not influence any aspect of the simulation, which will appear just as a simulation performed without this technology.

The principal stress distributions at different extrusion stages along the line AB (as shown in Fig. 6) are shown in Fig. 10. Compared with the longitudinal stress in paste extrusion, which is shown in Fig. 11, the distribution of the longitudinal stress in hot aluminium extrusion is different. As can be seen from Fig. 11, the stress is linear along the transverse direction when the extrusion ratio is high in paste extrusion, while it is totally different in the hot aluminium extrusion. It can also be seen from Fig. 10 that the maximum stress at the surface of the RUN 1 extrusion is higher than that of RUN 3, although the surface quality is much better in RUN 1.

Discussion of cracking criteria

If a criterion can explain the following four phenomena, then it can be regarded as effective in predicting the surface cracking which occurs in hot extrusion of aluminium alloy AA 2014.

1. Phenomenon 1 (P1): cracking occurs on the extrudate surface and is not seen at other locations.
2. Phenomenon 2 (P2): the extrusion suffers serious surface cracking during extrusion at high initial temperatures, such as in RUN 3. It is not a serious problem for extrusion at low initial temperatures.
3. Phenomenon 3 (P3): in some cases, for instance the RUN 2 extrusion used in this study, surface cracking occurs during the middle period of the process and becomes more serious as the process continues.
4. Phenomenon 4 (P4): the severity of cracking is less in the indirect mode than in the direct mode.

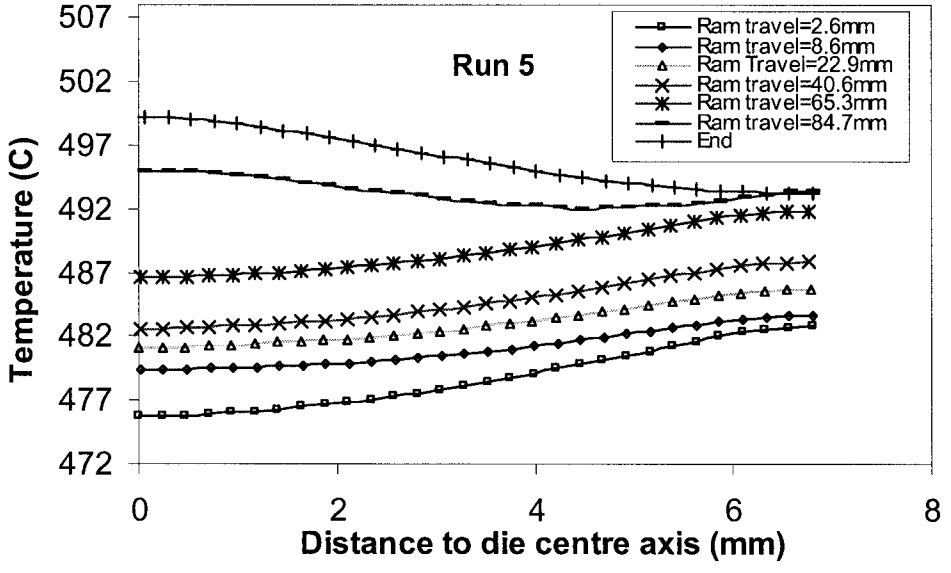

8 Temperature evolution of line A–B in extrusion run 5

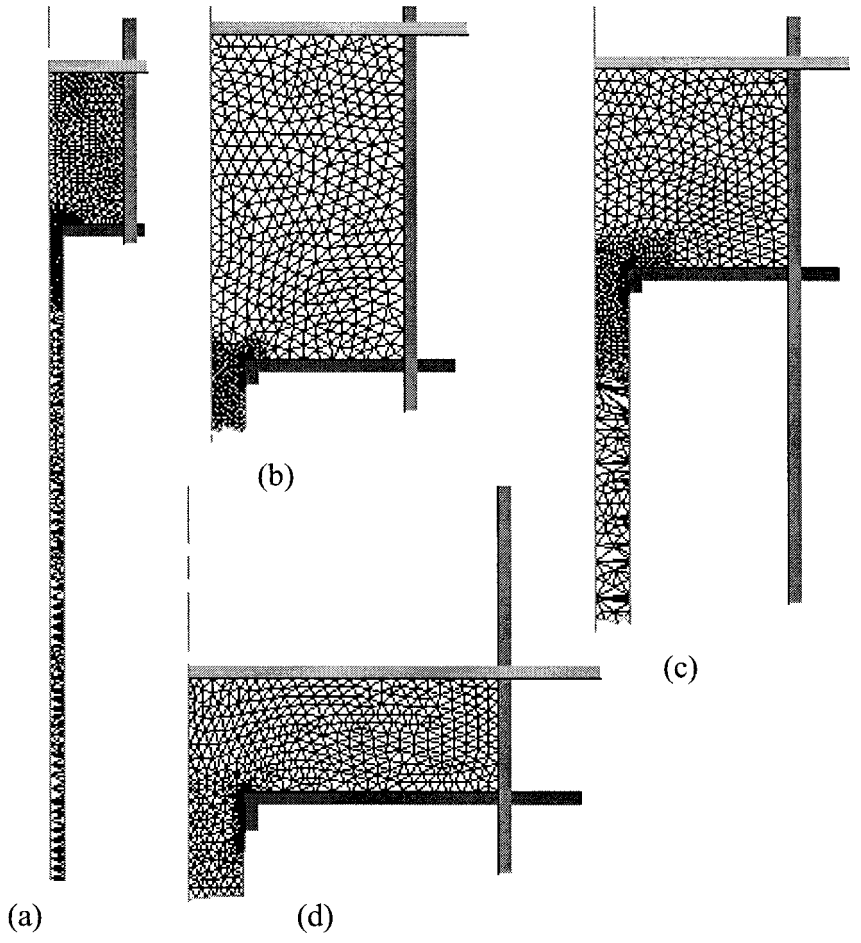

a before cut; *b* direct extrusion; *c* indirect extrusion; *d* end of direct extrusion

9 Cut technology

It should be recalled that a higher value of damage parameter, i.e. the C1–C6 mentioned above, indicates a greater chance of cracking. If the assumed 'critical value' does exist, then surface cracking will occur if the predicted value is higher than the 'critical value'.

PHENOMENON 1

As can be seen from Fig. 12*a*–*f*, all simulations, operating with different criteria, give the maximum predicted value on the extrudate surface, and the predicted value decreases smoothly from the surface to the centre of the extrudate. The

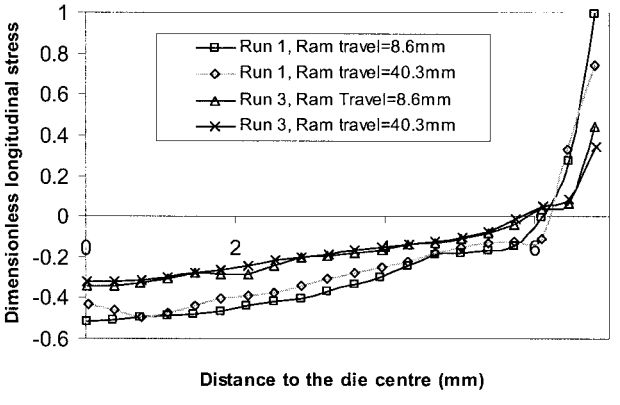

10 Principal stress distribution along line A–B at different stages of hot extrusion

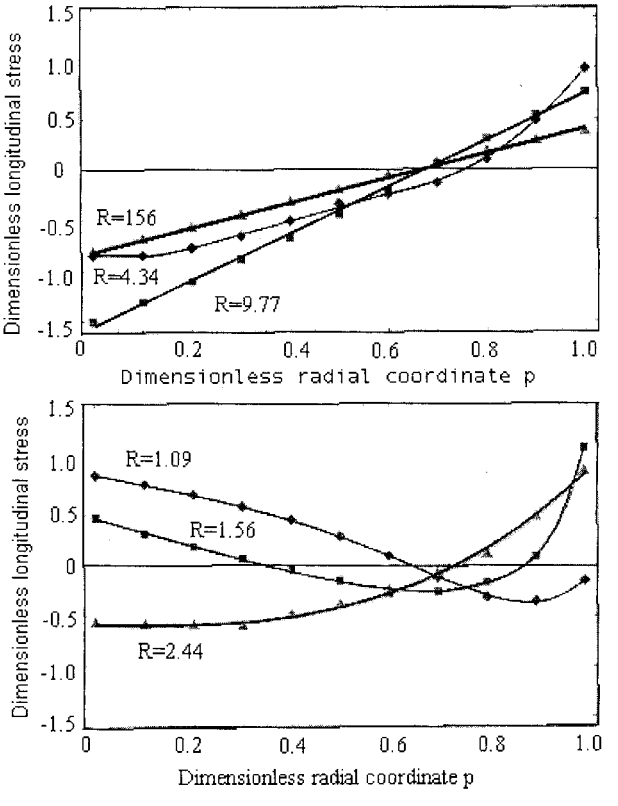

11 Principal stress distribution in transverse direction in paste extrusion at different levels of extrusion ratio *R* (Ref. 14)

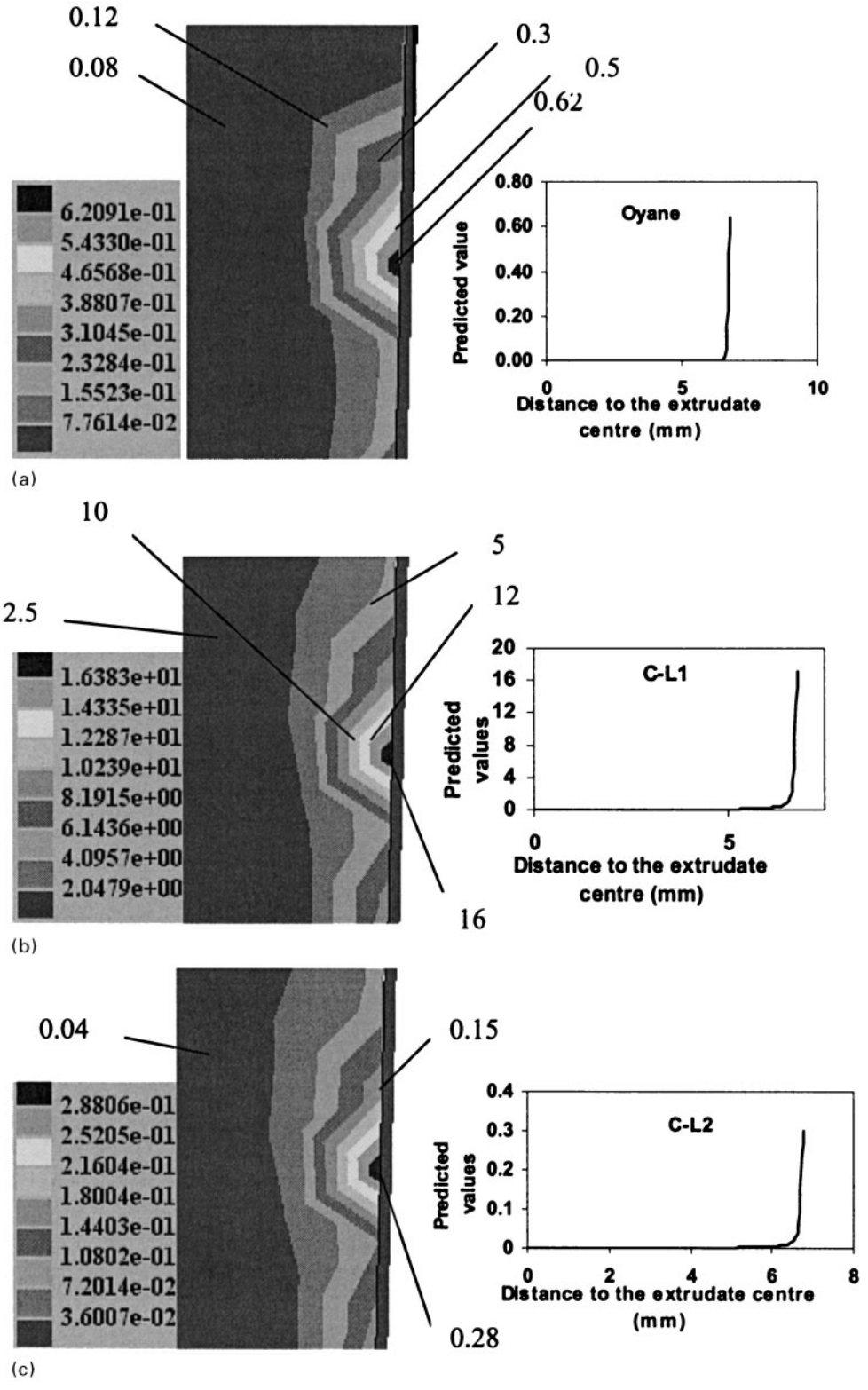

a Oyane; *b* C–L1; *c* C–L2; *d* Ayada; *e* GW; *f* instant *Z*; *g* surface cracking after crack function triggered

12 Predicted values of cracking criteria

maximum predicted values also begin to appear near the re-entrant die corner, which can be seen in Fig. 12*f*. It follows that if there is a critical value for the cracking criterion, then this value would be reached first on the surface, according to all of the criteria adopted in this study. This was illustrated after the crack function of the software was triggered, as can be seen in Fig. 12*g*. Hence we may conclude that all of the criteria are effective in predicting the first phenomenon.

PHENOMENON 2

However, as can be seen in Figs. 13–17, these criteria, except the temperature criterion, do not permit prediction of the second phenomenon. According to the criteria mentioned above, which all assume there is a critical value for surface cracking, the critical value should be reached first in the extrusion of RUN 3, which suffers the most surface cracking in the experiments. However, as can be

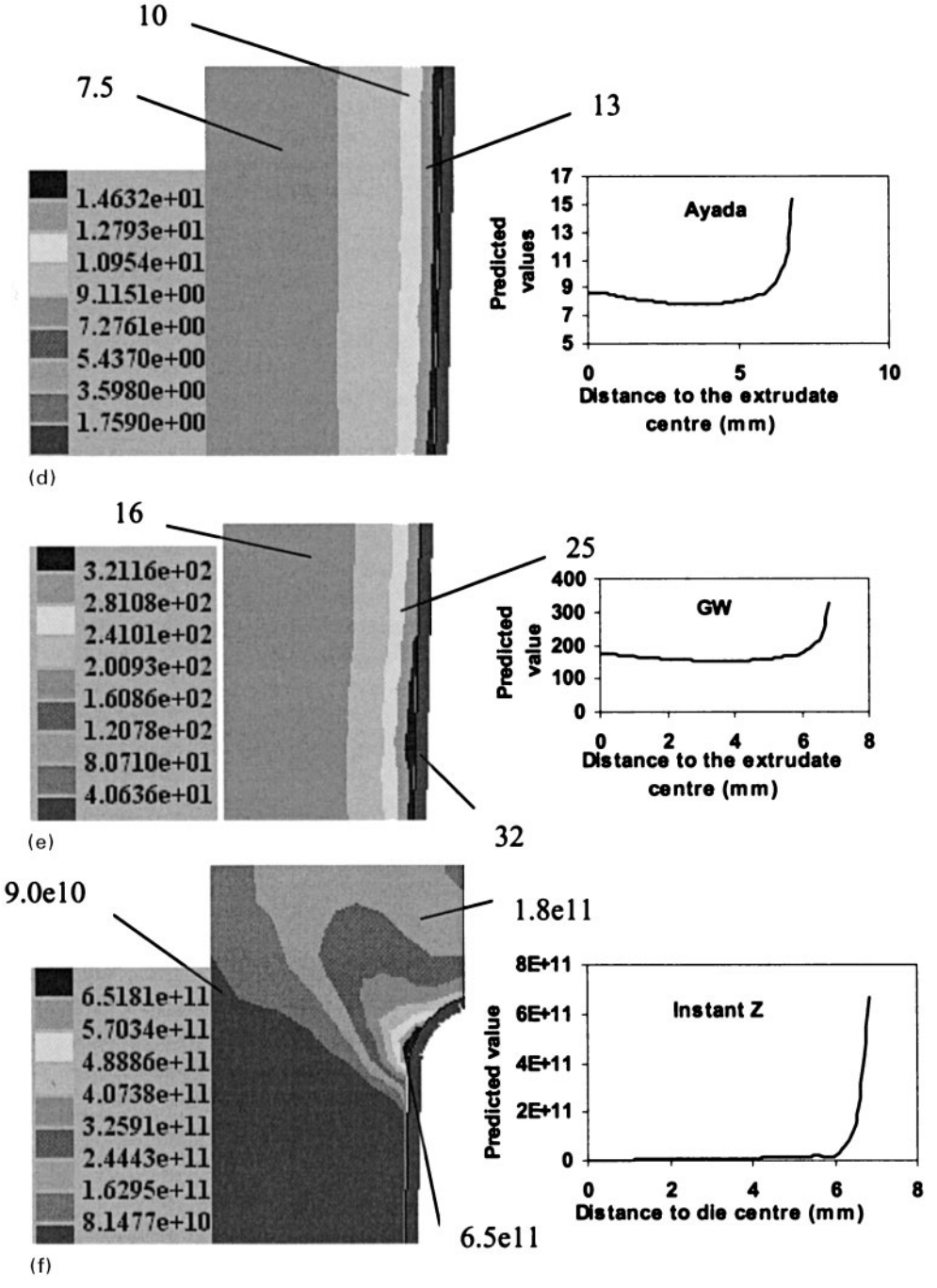

a Oyane; *b* C–L1; *c* C–L2; *d* Ayada; *e* GW; *f* instant *Z*; *g* surface cracking after crack function triggered

12 Predicted values of cracking criteria (cont.)

seen in Figs. 13–17, in which the Oyane, C–L, Ayada, and GW criteria are employed, the predicted value of RUN 3 is not the maximum among all the predicted values. The predicted curves of the different RUNs are convoluted and cannot be used to draw the conclusion that RUN 3 suffers most from surface cracking. Meanwhile, for the criteria of Ayada and GW, as can be seen in Fig. 13, the predicted curve of the RUN 1 extrusion has the highest position while this extrusion has the best surface quality in the experiments. In Fig. 17, the curve of RUN 3 is a little lower than the curve of RUN 2, while in experiments the surface cracking which happened in RUN 2 is less serious than that in RUN 3. The data shown in Figs 13–15 were extracted from line CD, as shown in Fig. 5, after the ram travelled the same distance. The data shown in Figs. 16 and 17 are extracted from the point D, as shown in Fig. 5.

PHENOMENON 3

It can be seen from Figs. 18–20 that the first three criteria, i.e. Oyane, C–L1, and C–L2 criteria, are valid. The predicted peak values at the middle of extrusion are higher than the maximum value at the beginning of extrusion. It can also be seen from Figs. 21 and 22, that the Ayada and GW criteria are obviously effective. The predicted values of these two criteria are continuously rising through out the extrusion, and this corresponds with the concept that if surface cracking occurs, it will become more and more severe as the process proceeds.

PHENOMENON 4

For the fourth phenomenon, it can be seen from Figs. 16 and 17 that the Ayada and GW criteria are valid. For the

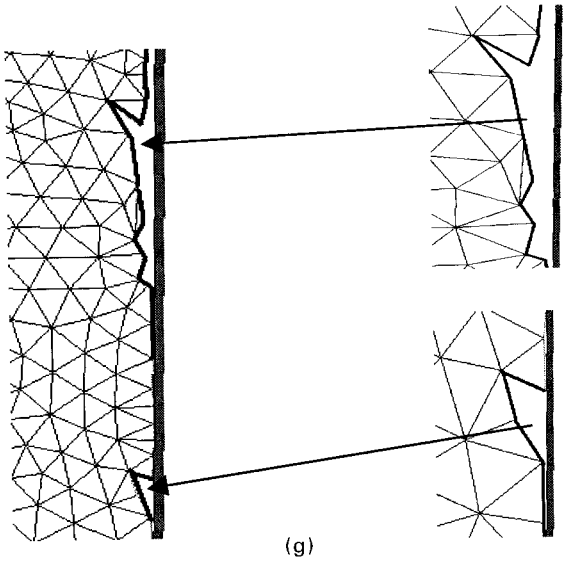

a Oyane; *b* C–L1; *c* C–L2; *d* Ayada; *e* GW; *f* instant *Z*; *g* surface cracking after crack function triggered

12 Predicted values of cracking criteria (cont.)

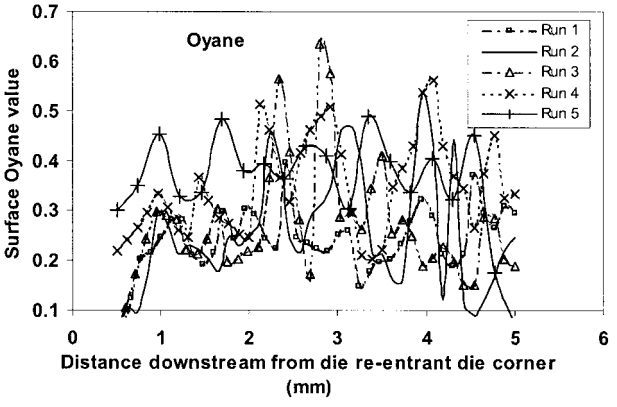

13 Simulation results using Oyane criterion

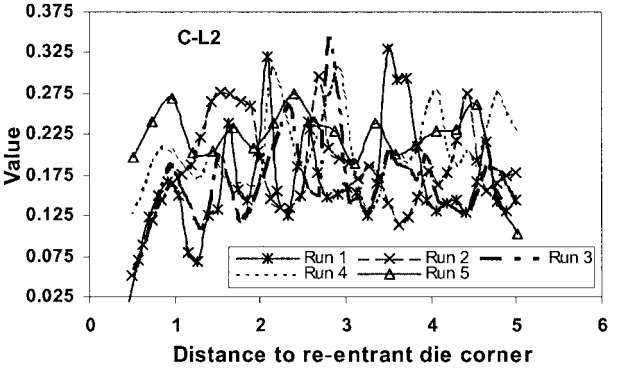

14 Simulation results using C–L2 criterion

simulation results of RUN 5, these two criteria give the predicted curve occupying the lowest position in the diagram.

The temperature criterion is also valid in explaining the fourth phenomenon, as can be seen from Fig. 7. It has been discussed previously that the temperature rise during extrusion results in incipient melting of the second phase particles, which form an intergranular network when rapidly quenched, resulting in a brittle product having poor mechanical properties.[16]

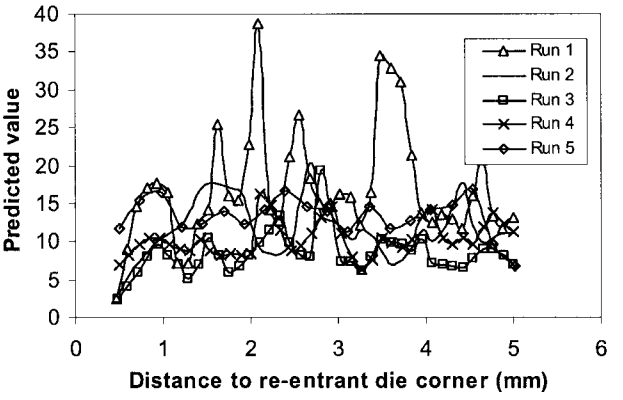

15 Simulation results using C–L1 criterion

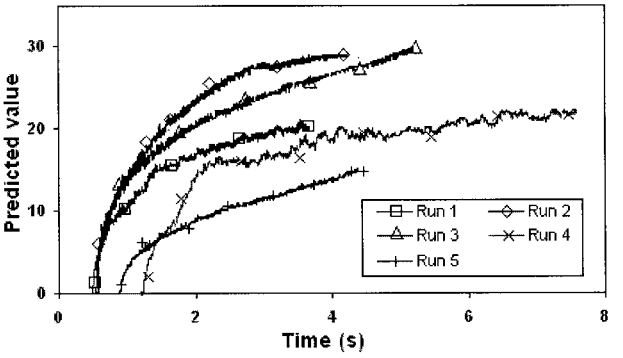

16 Simulation results using Ayada criterion

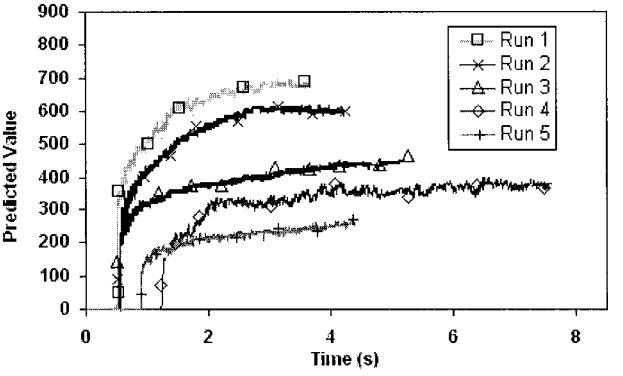

17 Simulation results using GW (Freudenthal) criterion

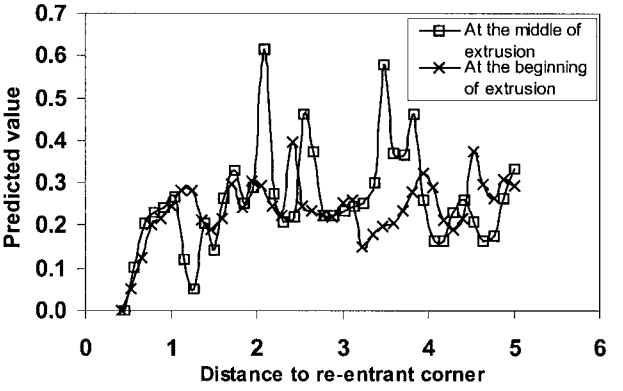

18 Predicted value of Oyane criterion at different stages

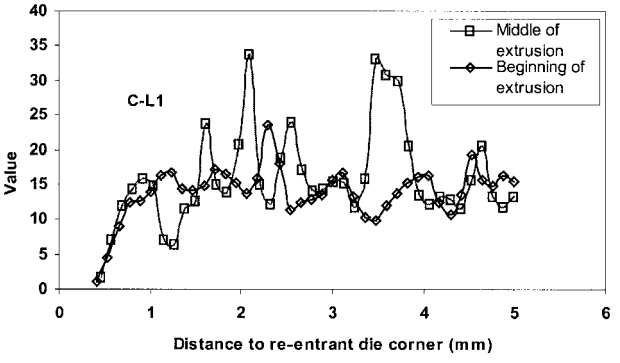

19 Predicted value of C–L1 criterion at different stages

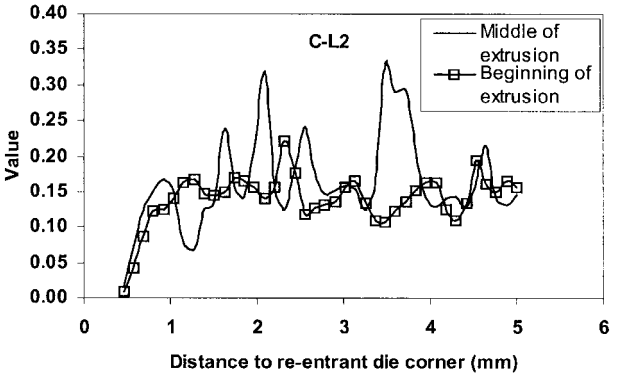

20 Predicted value of C–L2 criterion at different stages

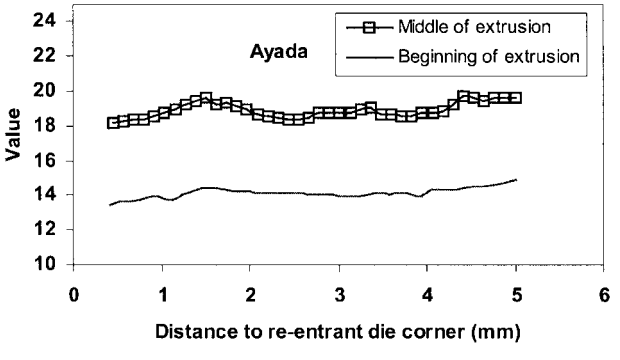

21 Predicted value of Ayada criterion at different stages

The other criteria are not effective in predicting the fourth phenomenon.

Discussion of the empirical criterion

Because the empirical method is regressed from all of the experiments, it is evident that it is effective in predicting the phenomena 1, 2, 4, and 5 mentioned above. Meanwhile, if only judged from the $\mathrm{Ln}(Z_i)$ value, it is difficult to predict if surface cracking will occur at the start of extrusion or part way through extrusion. However, with the FEM predicted value of $\mathrm{Ln}(Z_r)$, this problem can be solved, as discussed below.

It can be seen from Figs. 23–26 that the predicted $\mathrm{Ln}(Z_r)$ value rises sharply at the beginning of extrusion, and then

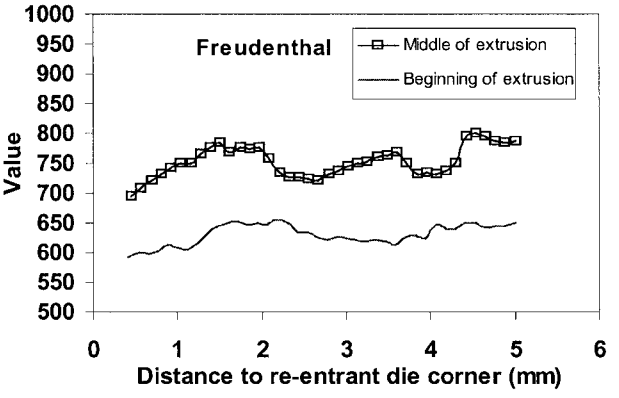

22 Predicted value of GW criterion at different stages

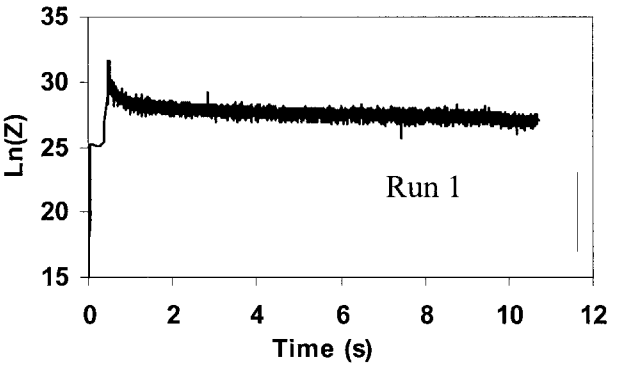

23 Predicted value of $\mathrm{Ln}(Z_r)$ in Run 1

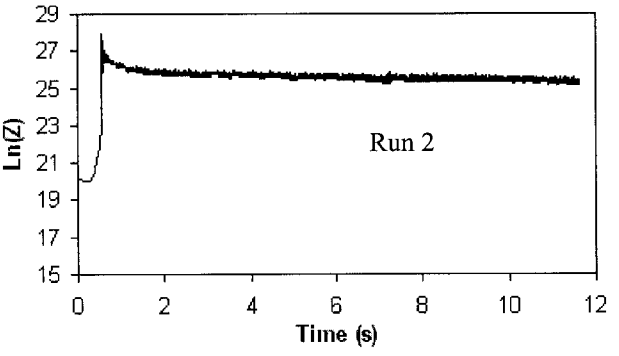

24 Predicted value of $\mathrm{Ln}(Z_r)$ in Run 2

Table 5 Comparison of Ln(Z) values

Extrusion code	Predicted peak value of $\mathrm{Ln}(Z_r)$	Predicted minimum value of $\mathrm{Ln}(Z_r)$	Initial value of $\mathrm{Ln}(Z_i)$	Critical value according to equation (17)
1	32·14	27·19	31·83	33·65
2	27·92	24·74	27·25	27·83
3	25·95	24·68	24·71	24·54
4	24·28	23·02	23·55	24·38
5	18·23	17·52		24·78

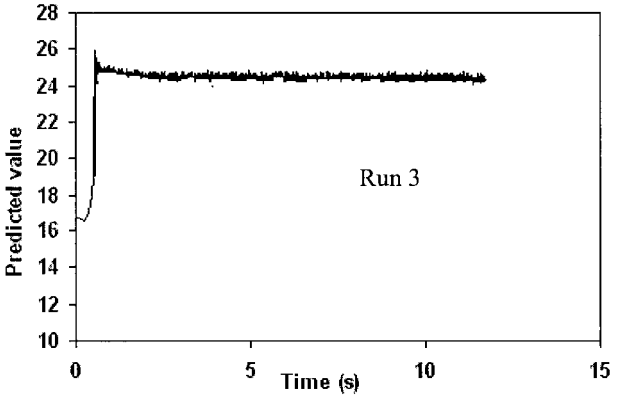

25 Predicted value of Ln(Z_r) in Run 3

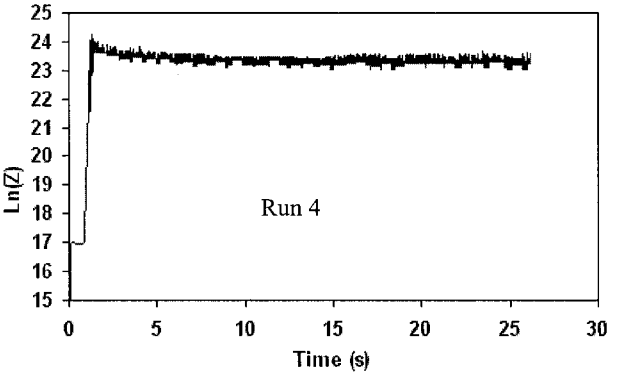

26 Predicted value of Ln(Z_r) in Run 4

decreases slowly throughout the remainder of the process. It is worth pointing out that the Ln(Z_r) – time curve is similar to the load – time curve, in which the peak value appears at the start of extrusion.

As shown in Table 5, for RUNS 1 and 4, the predicted instantaneous Ln(Z_r) value is lower than the critical value throughout extrusion. For RUN 2, as can be seen from Fig. 25, the predicted peak value is higher than the critical value at the start of extrusion but decreases to values lower than the critical value at later stages of extrusion. Figure 26 indicates that for RUN 3, the predicted value is higher than the critical value throughout extrusion. These experiments correspond to real situations: the surface quality remained good throughout the whole process for runs 1 and 4, while surface cracking occurred part way through extrusion in RUN 2, and at the start of extrusion in RUN 3.

It can be seen from these discussions that the combination of Ln(Z_i) and Ln(Z_r) enables surface cracking to be predicted. If Ln(Z_i) is higher than the critical value given by equation (19), then surface cracking will occur, and if Ln(Z_r) is higher than the critical value throughout extrusion, then the extrudate will suffer from surface cracking throughout extrusion.

Conclusions

The results are summarised in Table 6.

1. Surface cracking is closely related to the temperature rise during extrusion. If the heat generated near the die land area increases the local temperature above the solidus point, localised melting can occur, which can cause severe cracking of the surface. This conclusion is supported by many previous studies.[1,15,16]

2. Given a so called 'critical value' that depends on the initial condition but not assumed universal, the empirical criterion can also predict all five phenomena.

Table 6 Validity of cracking criteria

	Phenomenon			
Criterion	1	2	3	4
Oyane	√	X	√	X
C–L1	√	X	√	X
C–L2	√	X	√	X
Ayada	√	X	√	√
Freudenthal	√	X	√	√
Temperature	√	√	√	√
Empirical	√	√	√	√

√ effective; X invalid.

3. The other criteria (Oyane, C–L, Ayada, etc.) cannot successfully predict all four cracking mechanisms occurring in hot aluminium extrusion. Although they are capable of predicting some phenomena, all criteria except temperature and the empirical formula failed to predict phenomenon 2.

Recommendation for further work

In this study, all work was performed using axisymmetrical extrusion, however, the danger of cracking increases in shaped extrusion near the re-entrant corners. In sections containing ribs, for example, which is an extreme case, there is a danger of the rib disintegrating. If the shape factor λ, which is used in equations (13) and (14), is considered in surface cracking phenomenon then further simulation work is required to establish the initial cracking conditions. In this study, the FEM simulation tooling is fixed and this is obviously not the case in actual processes. More experiments and simulations with deformable dies are required if further conclusions are to be drawn.

References

1. T. SHEPPARD: 'Extrusion of aluminium alloys', Vol. 5, 205–245; 1999, Dordrecht, Kluwer Academic.
2. L. F. MONDOLFO, J. G. BARLOCK and A. P. TOMEO: *Energies: J. Solar Energ. Soc. Am.*, 1976, **2**, 365–386.
3. T. SHEPPARD: *Mater. Sci. Technol.*, 1993, **9**, 430–440.
4. R. HAMBLI and M. RESZKA: *Int. J. Mech. Sci.*, 2002, **44**, 1349–1361.
5. S. E. CLIFT, C. E. HARTLEY, N. STURGESS and G. W. ROWE: *Int. J. Mech. Sci.*, 1990, **32**, 1–17.
6. F. A. MCCLINTOCK, S. M. KAPLAN and C. A. BERG: *Int. J. Mech. Sci.*, 1996, **2**, 614–628.
7. M. OYANE, T. SATO, K. OKIMOTO and S. SHIMA: *J. Mech. Work. Technol.*, 1980, **4**, 65–79.
8. M. G. COCKCROFT and D. J. LATHAM: *J. Inst. Met.*, 1968, **96**, 2444–2477.
9. F. A. MCCLINTOCK, S. M. KAPLAN and C. A. BERG: *Int. J. Mech. Sci.*, 1966, **2**, 614–630.
10. T. SHEPPARD: *Mater. Sci. Technol.*, 1999, **15**, 459–463.
11. J. R. RICE and D. M. TRACEY: *J. Mech. Phys. Solids*, 1969, **17**, 201–218.
12. D. KO, B. KIM and J. CHOI: *J. Mater. Process. Technol.*, 1996, **62**, 166–174.
13. A. T. DOMANTI, D. J. HORROBIN and J. BRIDGEATER: *J. Mech. Sci.*, 2002, **44**, 1381–1410.
14. M. G. TUTCHER and T. SHEPPARD: *Met. Technol.*, 1980, **7**, 488–493.
15. S. J. PATERSON: 'The direct and indirect extrusion of aluminium alloys', Vol. 4, 262–280; 1981, London, London University.
16. T. SHEPPARD and R. P. VIEROD: *Mater. Sci. Technol.*, 1985, **1**, 321–324.

17. T. SHEPPARD and R. P. VIEROD: *Mater. Sci. Technol.*, 1987, **3**, 285–290.
18. I. FLITTA and T. SHEPPARD: *Mater. Sci. Technol.*, 2003, **19**, 23–24.
19. T. SHEPPARD: *Mater. Sci. Technol.*, 1999, **115**, 459–463.
20. R. J. DASHWOOD, H. B. MCSHANE and A. JACKSON: Proc. 6th Int. Seminar on 'Aluminium extrusion technology', Chicago, IL, May 1996, Aluminium Extruders Council, Vol. 1, 331–39.
21. X. DUAN and T. SHEPPARD: *Int. J. Mech. Sci.*, 2003, **44**, (10), 2155–2172.
22. I. VENAS, J. HERBERG and I. SKAUVIK: 'Aluminium technology '86', Proc. Int. Conf., Norway, 1986, Hydro Aluminium, 23–26.